Universal Journal of Green Chemistry
https://ojs.wiserpub.com/index.php/UJGC/

Research Article

Systematic Multivariate Analysis for Optimizing Active and Selective AuPd-Based-Nanocatalyts towards Benzyl Alcohol Oxidation

Miguel R. I. Guerra[1], Maitê L. Gothe[1], Adolfo L. Figueredo[1], Marcos V. Petri[1], Nágila Maluf[1], Anderson G. M. da Silva[2], Pedro Vidinha[1], Marco A. S. Garcia[3]*

[1] Department of Fundamental Chemistry, Institute of Chemistry, University of Sao Paulo, Av. Prof. Lineu Prestes, 748, Sao Paulo 05508-000, SP, Brazil
[2] Department of Chemical and Materials Engineering—DEQM, Pontifical Catholic University of Rio de Janeiro (PUC-Rio), Rua Marques de Sao Vicente, 225, Gavea 22451-900, Brazil
[3] Department of Chemistry, Federal University of Maranhao, Av. dos Portugueses 1966, Sao Luis 65080-805, Brazil
E-mail: marco.suller@ufma.br

Received: 22 March 2024; **Revised:** 29 June 2024; **Accepted:** 1 July 2024

Abstract: Supported bimetallic gold-palladium (AuPd) nanomaterials have been extensively studied as highly active and selective nanocatalysts for oxidation reactions. For long-term viability, optimizing synthesis and reaction parameters is essential for utilizing noble-based materials once they are expensive to produce on a large scale. For that reason, using a performance-focused strategy like a multivariate experimental design is an optimal solution for simultaneously investigating the effects of different parameters and implementing such materials in business activities. Therefore, herein, we report a systematic multivariate optimization of model AuPd/SiO_2 nanocatalysts for selective benzyl alcohol oxidation in solvent-free sustainable conditions, which allows for the evaluation of the impact of the material synthesis and reaction conditions on the process and optimization of reaction and calcination temperatures. Our multivariate analysis shows that the calcination temperature has considerably impacted the structural properties of gold nanoparticles; still, these changes did not produce a pronounced effect on the material's catalytic properties. On the other hand, the physical variables of reaction time and temperature had a more significant influence on both conversion and selectivity. An 18% conversion of benzyl alcohol with a benzaldehyde selectivity of 93% was achieved under a 562 °C catalyst calcination temperature, 100 °C reaction temperature, and 4 h of reaction time.

***Keywords*:** bimetallic catalysts, gold, palladium, benzyl alcohol, oxidation, multivariate design

1. Introduction

The gold (Au)-containing nanomaterials class is one of the most fascinating in current nanoscience, especially in catalysis [1–6]. After the discoveries of Haruta and Hutchings regarding gold catalytic properties [7–9]. Rossi and colleagues demonstrated that supported gold nanoparticles could be used to oxidize alcohols in the presence of a base, like the oxidation of ethane-1,2-diol, propane-1,2-diol, and ethylene glycol [10,11], which fairly advanced the catalytic applications of the metal. However, the limitations of using basic conditions, such as side reactions or catalyst deterioration, were soon noted [12,13]. Thus, a beneficial strategy to overcome such drawbacks was adding another metal as a co-catalyst, avoiding alkaline compounds; palladium (Pd) was the most common choice, making their use a standard practice [14–16]. In addition,

DOI: https://doi.org/10.37256/ujgc.2220244619

researchers realized that including a second metal improved the efficiency of Au-based catalysts, creating electronic and/or geometric synergetic effects advantageous to the catalytic process [17,18]. Then, several studies have used different Au/Pd ratios for the oxidation of alcohols in the presence of O_2, aiming at the activity and selectivity of the process [18–20]; on the other hand, other studies have shown that the addition of Pd as a second metal helps in its durability and reuse [21,22], once and for all proving the importance of the alloying of both elements. Therefore, using such metals for oxidation reactions and the recent advances in the field will soon not be restricted to academic practice.

In this context, there are many preparation options for metallic nanoparticles in a controlled manner, primarily based on the chemical reduction of a metallic precursor in the presence of a stabilizing agent, like PVA, L-hydroxyproline biomolecule, titanium isopropoxide, and CTAB [22–25]. Other experimental parameters, such as temperature, reduction time, and nature of the reducing agent, can also affect the catalytic process. The role of the stabilizing agent is critical since it modifies the surface energies of the nanoparticles during the growth stages, overcoming the thermodynamics limitations and allowing the obtaining of metallic nanoparticles with a particular shape. However, the presence of these stabilizing agents on the surface of the nanoparticles prevents their direct application in catalysis, where it is well established that having a clean surface is an indispensable requirement. Consequently, once the metal nanoparticles are prepared, they must inevitably be subjected to specific decontamination protocols to remove the presence, even in residual quantities, of the stabilizing agents on the surface of the nanoparticles [22,24,26].

The calcination method, besides being very accessible, gives good results in the removal of stabilizer agents in nanostructures [27–29], but it is still far from being a perfect methodology. The calcification of a nanostructured material can cause the aggregation of nanoparticles or change how the two metals are distributed on the particle, which can heavily influence catalytic activity and reaction selectivity [30,31]. Conversely, calcination of the catalyst will expose more nanoparticles by removing the residual stabilizing agent used in synthesis, thus increasing catalytic activity. Moreover, the temperature of the reaction often has a significant impact on conversion and selectivity rates. Despite the oxidation of alcohols to aldehydes being successfully catalyzed by AuPd bimetallic nanoparticles in the literature, it still often presents issues of activity and selectivity as more oxidized products are formed at higher conversion rates.

One commonly employed model reaction for this purpose is the oxidation of benzyl alcohol. Nowadays, it is carried out using several methodologies, which include gold supported on strontium surface-enriched $CoFe_2O_4$ nanoparticles ($Au/Sr(OH)_2/CoFe_2O_4$); tungstate supported on metal oxide ($H_3PW_{12}O_{40}/CeO_2$) using H_2O_2; Pd/CeO_2 catalyst; and bimetallic Pd-Fe catalysts supported on TiO_2 using H_2O_2 [32–35]. Previous reports on the oxidation of benzyl alcohol to benzaldehyde using Au/Pd catalyst on solventless conditions includes the study by Rossi and colleagues in 2013 [15], in which they obtained a conversion of 48.5% and 96.8% of selectivity to benzaldehyde, working with Fe_3O_4@SiO_2-NH_2-AuPd catalyst and reaction conditions, 2 bars of O_2, reaction temperature 100 °C and a 2232:1 relation substrate:metal. Subsequently, in 2019 [30], the same group conducted another study using the same catalyst and substrate:metal relation; they obtained approximately 80% conversion and 90% selectivity in 60 min of reaction time, 100 °C, and 6 bar of O_2. Saiman et al. [14], performed the oxidation of benzyl alcohol without using solvents; instead, they used H_2O_2 as an oxidant. These authors demonstrated that this approach was viable, obtaining conversions of around 10% and selectivities of 90% of benzaldehyde. Also, Moura and colleagues in 2019 [32], using the $Au/Sr(OH)_2/CoFe_2O_4$ catalyst, reached 58% of conversion with 76% of selectivity to benzaldehyde.

In this context, it is clear that the advance in gold-based catalysts has shown remarkable progress that might be industrially available soon; however, considering that the design of heterogeneous catalytic systems is usually a complex task, a promising strategy for the correlation among all the parameters mentioned above has been progressively employed to help scientific investigations: a multivariate analysis. In this case, experimental design is a useful mathematical tool for rationalizing the combined effect of independent variables on a particular process, as it can generate equations that express the impact of an operating parameter such as temperature on a responsive variable, for instance, conversion and selectivity.

Targeting to achieve an equilibrium between the usual trial-and-error strategy and the rational "design" approach to produce and investigate catalytic activities, we report a multivariate design to prepare/investigate the key parameters that may affect the catalytic activities of AuPd nanoparticles and optimize both activity and selectivity towards the benzyl alcohol oxidation as a model reaction. To this end, AuPd core-shell nanoparticles were employed as a model active phase, while silica was used as an inert inorganic support. Then, to accomplish this, we evaluated the impact of the catalyst

synthesis and reaction condition on the oxidation of benzyl alcohol by multivariate analysis, which is a necessary chore for process optimization.

2. Experimental

2.1 *Materials*

The following metal precursors and chemical reagents were purchased from Sigma-Aldrich (São Paulo, Brazil) and used as received: $HAuCl_4$ (tetrachloroauric) acid (aqueous solution 30% m/m); NaOH (sodium hydroxide); PVP (polyvinylpyrrolidone 55,000 g mol^{-1}); K_2PdCl_4 (potassium tetrachloropalladate); $Na_3C_6H_5O_7$ (sodium citrate); hydroquinone; acetone; dichloromethane; benzyl alcohol; benzoic acid; benzaldehyde; benzyl benzoate; benzene; biphenyl; silica 99.8% HDK-T40. The gases used for the operation of the analytic equipment (argon, synthetic air, acetylene, nitrogen, and carbon dioxide) and used in reactions (oxygen) were acquired from the company Gama Gases (São Paulo, Brazil) in ultrapure form.

2.2 *Synthesis of Au@Pd nanoparticles*

To obtain the Au@Pd catalyst, we followed a two-step synthesis procedure based on previously modified reported procedures[36,37]. First, gold seed nanoparticles were synthesized by adding 2 mL of tetrachloroauric acid (25 mM) to 15 mL of water, stirring the solution at 415 rpm in a 50 mL flask. After 5 min, 378 µL of NaOH (465 mM) were added, followed by the addition of water to reach a total volume of 20 mL. The flask was then placed in an oil bath at 115 °C for 20 min under reflux until the reaction mixture began to boil. Subsequently, 600 µL of a sodium citrate solution (50 mg mL^{-1}) were added. After 10 min, the reaction changed to a dark blue and then to a deep red, indicating completion. The gold seed nanoparticles were cooled to room temperature and stored as is.

To synthesize Au@Pd nanoparticles, 10 mL of the as-prepared Au seeds were mixed with 96 mL of PVP (0.1%) and 15 mL of water. The mixture was heated under magnetic stirring in an oil bath at 50 °C for 10 min. Then, 6 mL of hydroquinone solution (30.0 mM) were added and stirred for over 10 min. Subsequently, 4.00 mL of K_2PdCl_4 solution (12.0 mM) were quickly added to the mixture. The reaction continued for 1 h, during which the clear red color transitioned to a reddish-brown and finally to black. The final product was cooled to room temperature. Multiple batches of the same reaction were prepared separately to yield sufficient mass of Au and Pd for catalytic reactions and material characterization. For example, to achieve a desired mass of 76.6 mg of Pd, 15 separate batches were prepared simultaneously, resulting in approximately 1.8 L of suspension. The suspension was then concentrated through several centrifugation steps. Initially, 300 mL of the suspension was divided into six 50 mL conical tubes and centrifuged at 7580 rpm (Eppendorf Centrifuge 5430, rotor F-35-6-30, São Paulo, Brazil) for 10 min. The supernatant was diluted and returned to the original suspension. The pellet was sonicated and transferred into 1.5 mL plastic tubes. This process was repeated until no visible pellet remained. Subsequently, the 1.5 mL tubes were centrifuged at 17,500 rpm for 10 min (rotor FA-45-24-11-HS), and the clear supernatant was discarded. The pellets were resuspended in water with a final volume of 3 mL.

2.3 *Synthesis of Au@Pd/SiO_2*

Typically, 300 µL of the suspension was dropped onto 750 mg of commercial SiO_2 in a Petri dish on top of a heating plate at 40 °C and homogenized with a spatula. This process was repeated until all the suspension was incorporated to obtain a 1% m/m catalyst in terms of Pd. The material was dried overnight at 80 °C under a vacuum and named ‘as-prepared catalyst’.

2.4 *Characterization techniques*

The percentage of Au and Pd metals in the Au-Pd/SiO_2 catalyst was determined by flame atomic absorption spectroscopy on a Shimadzu AA-6300 spectrometer (São Paulo, Brazil). The XRD analysis was performed in a Rigaku

Miniflex (São Paulo, Brazil) with Cu Kα radiation (λ = 15,418 A0) at 2θ in the range 10°–80°. Superficial area and pore volume were obtained on Quantachrome Nova 1200e equipment (São Paulo, Brazil) using the BET and BJH calculation methods, respectively. The sample was degassed at 110 °C under vacuum for 14 h before the N_2 adsorption/desorption measurements. Transmission electron microscopy (TEM) images were obtained in a Jeol JEM 2100 microscope (São Paulo, Brazil) at 200 kV voltage, with a LaB6 filament gun and a high-resolution annular dark field (HAADF) detector with a resolution of 0.23 nm (dot) and 0.14 nm (network). The reaction products were analyzed using a Shimadzu gas chromatograph (São Paulo, Brazil) with a flame ionization detector (CG-FID). An example chromatogram can be found in Supplementary Material (Figure S5). The column used for product analysis was RTX-Wax (30 m × 0.25 mm × 0.25 mm), and biphenyl was used as an internal standard.

2.5 *Catalytic oxidation of benzyl alcohol*

The reactions were carried out in a Fisher-Porter (São Paulo, Brazil) glass reactor. A mass of 10 mg of catalyst was subjected to a pre-reduction under 5 bars of H_2 for 30 min at 100 °C before the reaction unless otherwise specified. The reaction time was initiated by adding benzyl alcohol to the pre-treated catalyst in a 5000:1 molar ratio of substrate to active metal and pressurizing the reactor with 2 bars of O_2. The reaction system was maintained at the set temperature and stirred at 600 rpm for 4 h.

2.6 *Multivariate experimental design*

The synthesized catalyst Au-Pd/SiO_2 was calcined at various temperatures, and the temperature of the benzyl alcohol oxidation reaction was also varied to construct a 2^2 central composite design with 3 replicates at the center, totalizing 11 experiments. In this central composite design, we considered calcination temperature independent variables, analyzed in the range 200–500 °C and reaction temperature 60–120 °C. The impact of these variables on benzyl conversion and selectivity towards benzaldehyde was evaluated. To that intent, eleven experiments were performed: 3 at the central point conditions (350 °C calcination, 90 °C reaction temperature) and 4 alpha points, with calcination and reaction temperatures, respectively α1: 138 °C, 90 °C; α2: 562 °C, 90 °C; α3: 350 °C, 48 °C; α4: 350 °C, 132 °C and 4 points corresponding to the simple factorial design, as seen in Supplementary Material (Table S1). The calcination was performed using a furnace (EDG Equipamentos, EDG3P-S, São Paulo, Brazil) under air for 2 h at the designated temperature, with a heating ramp of 10 °C min^{-1}. Statistica software 10.0 (TIBCO Software Inc, USA), was used to calculate each independent variable's effects and obtain a response surface.

3. Results and discussion

The investigations started with the synthesis described in the experimental methods section; the AuPd/SiO_2 was obtained as a model heterogeneous catalyst, in which a multivariate design was employed for investigating the key parameters that may affect the catalytic activities of AuPd/SiO_2 in an attempt to optimize both activity and selectivity towards benzyl alcohol oxidation. The mass percentage of each metal in the obtained catalyst was 2.09% m/m of Au and 1.32% m/m of Pd, as evaluated by atomic absorption spectrometry, which equals a molar ratio of Au:Pd of 1:1.17. As seen in Supplementary Material Table S2, both the BET surface area and the pore volume of the calcined catalyst are smaller than those of the as-prepared catalyst, which is in line with similar materials reported in the literature [31]. This points to efficient removal of the residual stabilizing agent PVP by heating under air, which could lead to higher catalytic activity due to better exposure of the nanoparticles to the substrate. The carbon content was evaluated by CHN elemental analysis as 0.42% in the as-prepared catalyst and 0.11% in the calcined catalyst.

TEM images of the as-prepared AuPd/SiO_2 catalyst and the calcined one are shown in Figure 1. Spherical nanoparticles of AuPd were observed at the surface of the silica support, averaging 17 nm in diameter in the as-prepared catalyst and 21 nm in the calcined one. As seen on the TEM images, the calcination process caused a slight increase in the average size

of the nanoparticles and a decrease in the BET surface area, probably due to sintering processes at higher temperatures. Histograms of nanoparticle size distribution can be found in Supplementary Material Figure S1.

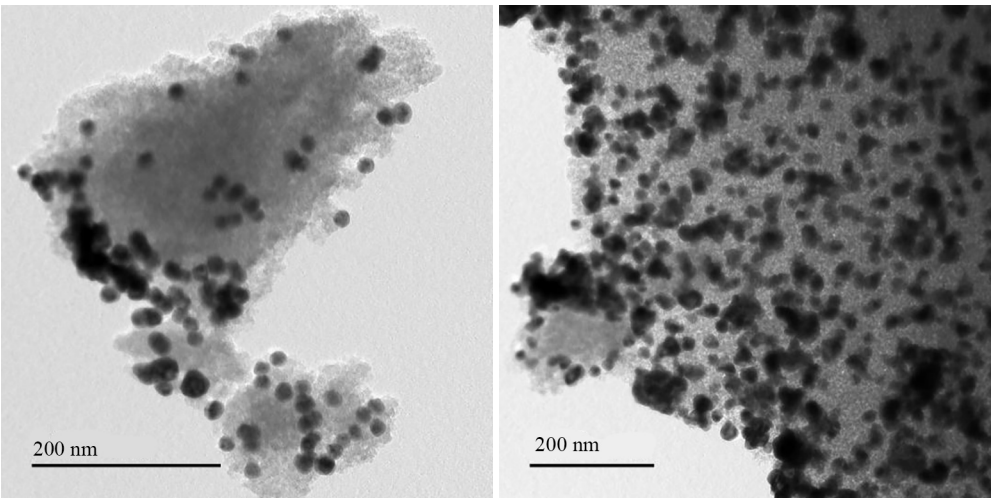

Figure 1. TEM images of $AuPd/SiO_2$. The as-prepared catalyst is on the left, and the catalyst calcined at 562 °C on the right image

The as-prepared $AuPd/SiO_2$ catalyst is composed of metallic nanoparticles, as shown by the XRD diffractograms for the $AuPd/SiO_2$ catalyst (Supplementary Material Figure S2A). The as-prepared catalysts displayed diffraction peaks that match the reference peaks for the pure Au fcc phase (ICSD 611623) and a shoulder dislocated towards the Pd fcc phase reference peaks (ICSD 648674). As shown in (Supplementary Material Figure S2B), after the calcination process, segregation of the PdO phase (ICSD 24692) could be observed, along with the appearance of peaks related to the $Au_{1.51}Pd_{0.49}$ alloy (ICSD 197459). The catalyst calcined at 562 °C and subsequently reduced with H_2 at 100 °C does not present PdO peaks in its XRD, but peaks consistent with the pure metallic Pd phase are noticed in addition to the AuPd intermetallic compound, which continues to be observed in Supplementary Material (Figure S2C). Therefore, the XRD pattern of the catalysts shows that the calcination process has changed the structure of the as-prepared catalyst, favoring the alloying of composing metals, ordering them in the intermetallic compound $Au_{1.51}Pd_{0.49}$, while also segregating Pd due to oxidation to PdO. Neither of the changes in structure has been reversed by subsequent reduction with H_2 since pure metallic Pd is still observed along with the $Au_{1.51}Pd_{0.49}$ peaks.

The as-prepared $Au@Pd/SiO_2$ catalyst contains Au and Pd in a 1 to 1.17 molar ratio, verified by atomic absorption spectrometry. Yet, its XRD pattern only reveals Au peaks, consistent with a core-shell structure where the Pd atoms are in a shell layer that is too thin or not crystalline enough to be observed by X-ray diffraction later[30]. Meanwhile, the calcined $AuPd/SiO_2$ sample presents diffraction patterns consistent with an $Au_{1.51}Pd_{0.49}$ alloy and pure metallic Pd, indicating that, if a core-shell structure was indeed formed from synthesis, it was disturbed by the calcination process.

The XPS analyses of the $AuPd/SiO_2$ catalyst (Figure 2 and Table 1) reveal that the surface of the as-prepared catalyst contains a much smaller amount of Au than of Pd (8.71 at.% Au and 91.29 at.% Pd). The XRD pattern of the as-prepared sample, in turn, mainly showed that Au crystallites were present. The combination of these analyses suggests that the as-prepared $Au@Pd/SiO_2$ catalyst was in the form of an Au core with a thin Pd shell. The XPS of the calcined catalyst shows that the thermal treatment exposed a larger percentage of Au (30.99 at.% Au and 69.01 at.% Pd) and oxidized Pd. Metallic Pd is present along with Pd in its oxide form in the XPS analysis of the calcined catalyst, but this could be due to the reduction of PdO by the technique. The reduction of the calcined catalyst by thermal treatment under H_2 did not significantly impact the % m/m of surface Au and Pd, which agrees with the results observed by XRD.

After synthesizing the $AuPd/SiO_2$ catalyst, we focused on the multivariate design of AuPd-based catalysts displaying desirable activity for selective benzyl alcohol oxidation. To this end, we have evaluated the impact of the catalyst synthesis and reaction conditions on the oxidation of benzyl alcohol, which was chosen as our reaction model.

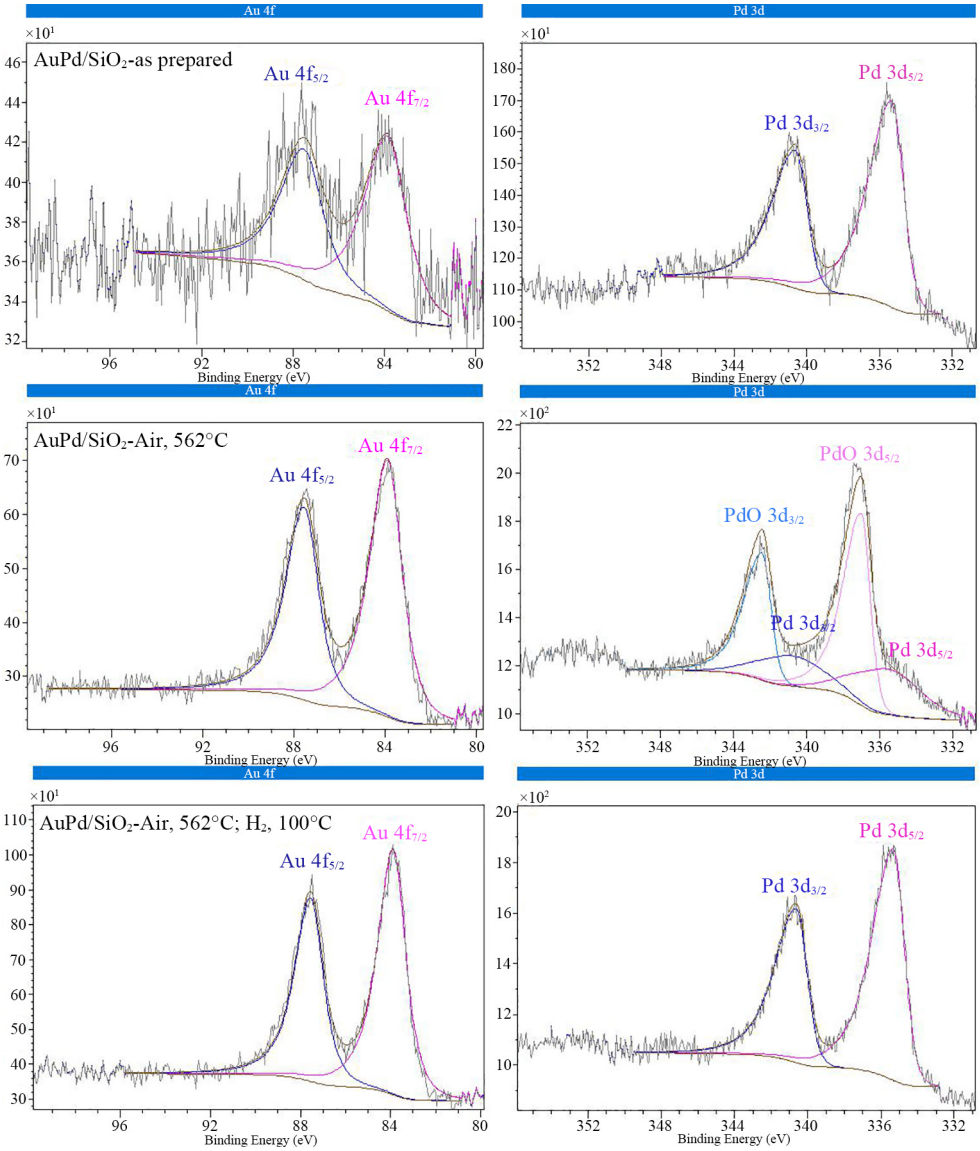

Figure 2. XPS Spectra of the AuPd/SiO_2 catalyst. The top spectra correspond to the as-prepared catalyst. Middle spectra refer to the catalyst subjected to calcination at 562 °C. The bottom images are relative to the catalyst submitted to calcination at 562 °C and subsequent reduction under the H_2 atmosphere

Table 1. XPS of the AuPd/SiO_2 catalyst

Catalyst	%At AuPd			BE /eV
As-prepared	Pd 3d	91.29	Pd $3d_{5/2}$	335.29
	Au 4f	8.77	Au $4f_{7/2}$	83.84
Air, 500 °C	Pd 3d	69.01	Pd $3d_{5/2}$	335.59
			PdO $3d_{5/2}$	336.99
	Au 4f	30.99	Au $4f_{7/2}$	83.90
Air, 500 °C; H_2, 100 °C	Pd 3d	70.54	Pd $3d_{5/2}$	335.30
	Au 4f	29.46	Au $4f_{7/2}$	83.88

A central composite design used the reaction and temperature at which the catalyst was calcined as independent variables. Their impact on benzyl alcohol conversion and selectivity to benzaldehyde was evaluated. The calcination temperature was studied from 200 to 500 °C, with 138 and 562 °C as alpha points, and the reaction temperature varied from 60 to 120 °C, with 48 and 132 °C as alpha points. A reaction time of 4 h was used in all experiments.

The Pareto chart in (Supplementary Material Figure S3) shows that, although both reaction and calcination temperature are significant to the conversion of benzyl alcohol, the influence of calcination temperature is rather small compared to the effect of reaction temperature. Both variables have a positive correlation to the transformation of benzyl alcohol in the linear and quadratic parameters. It can also be noted that the combined effect of the reaction and calcination temperatures is weak, meaning they are independent of each other.

When evaluating the effects of reaction and calcination temperatures on the selectivity of benzyl alcohol oxidation to benzaldehyde, only the reaction temperature could be considered significant. In contrast, the impact of calcination temperature on selectivity is lower than that of the experimental error, as seen on the Pareto chart (Supplementary Material Figure S4). Because the experimental error is low, the calcination temperature can be assumed not to affect selectivity at 4 h of reaction. On the other hand, the reaction temperature significantly negatively impacts the selectivity of the partially oxidized product, benzaldehyde, both in the linear and the quadratic effects.

A variance analysis was performed on the responsive variables of conversion and selectivity to evaluate the experimental error and the fitting of the model. The random error, resulting from experimental procedures, is observed to be relatively low (0.078 in conversion and 2.329 in selectivity), which excludes any contribution of the experimental error to a possible lack of fit of the predictive model. Moreover, the comparison between the residual errors and regression errors has shown that the residual error is much lower than the regression error for both variables, which means that the model can be used to fit experimental data. Regression coefficients R^2 of 0.99 and 0.93 were obtained, configuring a great fit of the model to the responses observed in the catalytic reactions. The ANOVA tables for the benzyl alcohol conversion and benzaldehyde selectivity analysis can be found in Supplementary Material (Tables S3–S6).

An empirical correlation between the dependent variables (conversion and selectivity) and independent variables (temperatures of reaction and calcination) is described in Equations (1) and (2), wherein the models were generated by the regression coefficients obtained in the statistical analysis of the factorial design.

$$Conversion = -3.4Tr + 2.4 \times 10^{-2}Tr^2 - 3.8 \times 10^{-2}Tc + 4.1 \times 10^{-5}Tc^2 + 1.5 \times 10^{-4}TrTc + 120 \quad (1)$$

$$Selectivity = 1.5Tr - 1.0 \times 10^{-2}Tr^2 + 41.7 \quad (2)$$

$$Tr = Reaction\ temperature$$

$$Tc = Calcination\ temperature$$

The mean quadratic regression evaluated the model's fitness and mean residual regression (F) ratio, which equals 95.15 and 54.69 in the conversion and selectivity models, respectively. Comparing the tabled F value of the Snedecor distribution to the respective degrees of freedom at the designated confidence level ($F_{0.95:5,5}$ = 5.05) for conversion and ($F_{0.95:2,8}$ = 4.46) for selectivity, the calculated values were more significant than the tabled values, meaning that the models are considered substantial and valid for predictive use. Nevertheless, the lack-of-fit and the pure-error ratio are greater than the tabled value ($F_{0.95:3,2}$ = 19.16) for conversion, which indicates that this model cannot be extrapolated to values beyond those used as the maximum and minimum levels of the factorial design.

The response surface graphs of benzyl alcohol conversion (Figure 3) and benzaldehyde selectivity (Figure 4) show the optimal reaction and calcination temperature ranges to maximize those variables in the response surface graph for benzyl alcohol conversion. A higher reaction temperature is observed to promote a higher conversion rate. However, the surface response graph for benzaldehyde selectivity shows that the reaction temperature should be low to achieve a selectivity of 88% benzaldehyde or higher. Interestingly, the calcination temperature, as seen in the Pareto chart, weakly influences both response variables.

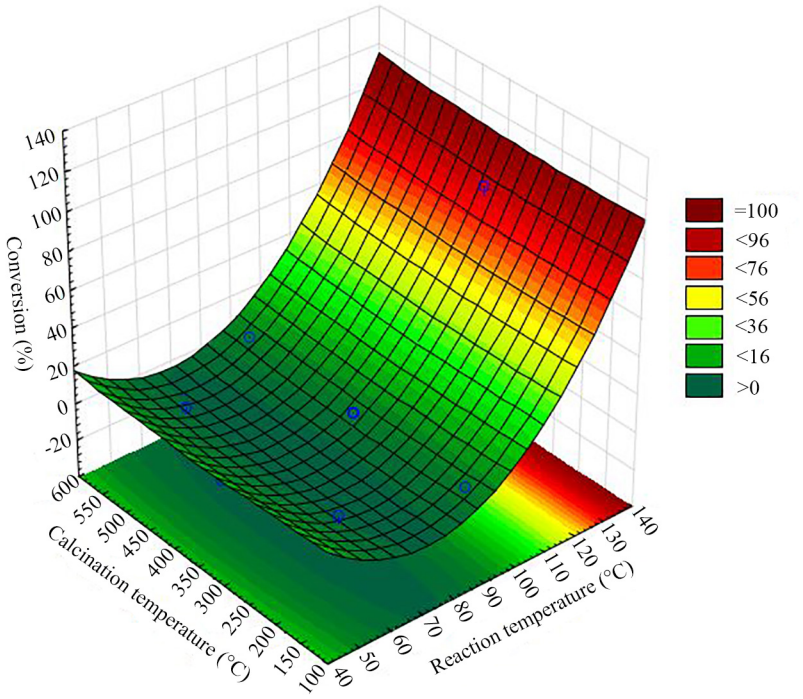

Figure 3. Fitted surface for conversion of benzyl alcohol as a function of reaction and calcination temperature

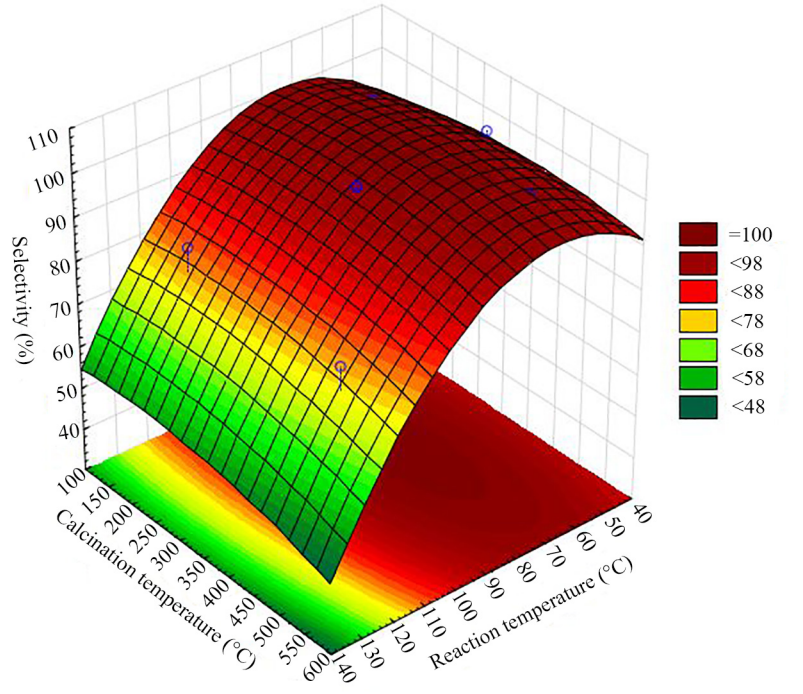

Figure 4. Fitted surface for selectivity of benzyl alcohol as a function of reaction and calcination temperature

The experimental design revealed that higher reaction temperatures are fundamental to achieving a satisfactory conversion rate for benzyl alcohol but are harmful to the process selectivity. Therefore, to better explore the selective

production of benzaldehyde, kinetic studies were performed at 120 °C, and the reaction time was extended to 6 h. Concerning the calcination temperature, the experimental design suggests that the calcination of the catalyst does not affect selectivity and has a slight positive effect on conversion. Thus, to better understand the role of catalyst calcination in this reaction, the kinetic analysis was repeated for the catalyst calcined at 562 °C and the as-prepared catalyst.

Figure 5 shows a kinetic graph of the benzyl alcohol oxidation reaction catalyzed by the as-prepared or calcined at 562 °C $AuPd/SiO_2$ material.

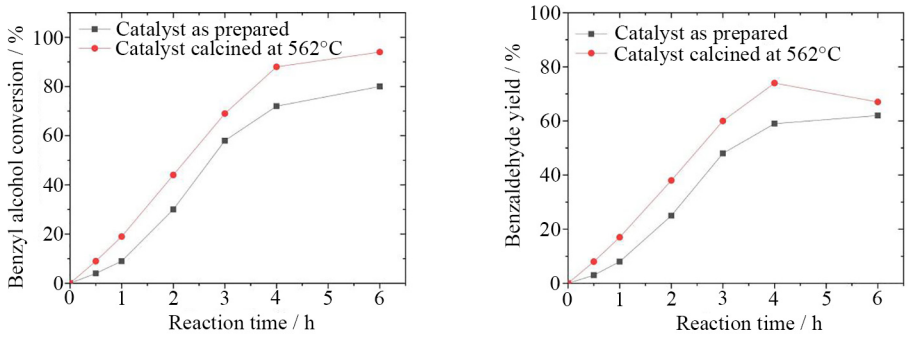

Figure 5. Benzyl alcohol conversion (**left**) and benzaldehyde yield kinetic (**right**) over $AuPd/SiO_2$ catalyst, both as-prepared and calcined at 562 °C. Reaction conditions: 2 bars of O_2, 50 mg of catalyst, and 5000:1 molar substrate to active metals ratio. Pre-treated in situ with H_2 at 100 °C.

While both catalysts have reached high conversion rates, the calcined catalyst performs better, following the results obtained from the experimental design. Nevertheless, at 6 h of reaction, the calcined catalyst shows a drop in benzaldehyde yield due to a sharp decrease in selectivity, surpassing the increase in conversion. Figure 6 shows how the yield of each oxidation product of benzyl alcohol evolves with reaction time. After up to 4 h of reaction, the calcined catalyst is still the better option for selective oxidation of benzyl alcohol to benzaldehyde. A longer reaction time leads to a slight increase in conversion and is detrimental to selectivity. Both the as-prepared and the calcined catalysts show a decrease in selectivity to benzaldehyde at longer reaction times in favor of more oxidized products. In particular, benzoic acid reaches 20% selectivity at 6 h of reaction time when the calcined catalyst is used, while when the catalyst is employed as-prepared, it only reaches 10%. Benzyl benzoate and benzene are also observed as products, although both maintain low selectivity values throughout the reaction.

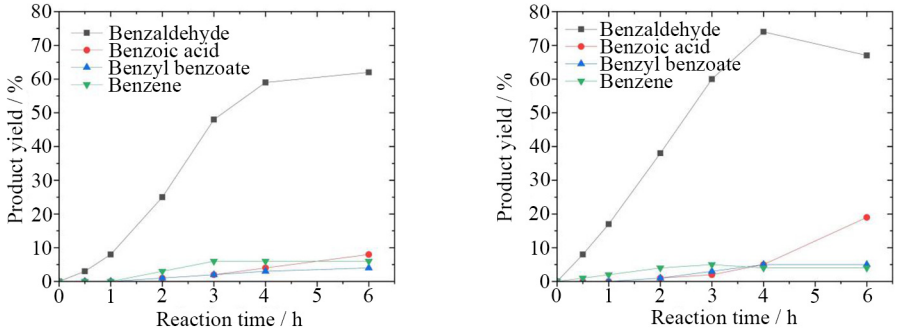

Figure 6. Product yield of benzyl alcohol oxidation catalyzed by $AuPd/SiO_2$, both as-prepared (**left**) and calcined at 562 °C (**right**). Reaction conditions: 120 °C, 2 bar of O_2, 50 mg of catalyst, and a 5000:1 molar ratio of substrate to active metals. Pre-treated in situ with H_2 at 100 °C.

4. Conclusions

AuPd nanoparticles anchored on SiO_2 were successfully synthesized as model catalysts for the selective oxidation of benzyl alcohol. The nanocatalysts were characterized by BET, TEM, XRD, and XPS to confirm their surface, structural, and textural composition. The experimental design suggested that the reaction temperature had the most significant effect on benzyl alcohol conversion. An 18% conversion of benzyl alcohol, with 93% selectivity towards benzaldehyde, was attained using a catalyst calcined at 562 °C, with a reaction conducted at 100 °C for 4 h. Also, the obtained results revealed that the calcination process of the as-prepared catalyst was essential to remove organic additives from the nanoparticle synthesis, which caused a significant disturbance of the bimetallic nanoparticle structure.

Nevertheless, the yield of the desired product was only slightly impacted by the calcination process. The physical reaction time and temperature variables proved much more critical, showing that the synthetic approach could produce high-quality nanoparticles. Such results are vital once it is necessary to know better how the advances in academic studies would apply better in future industrial applications, and reflections regarding their best performance are essential and are part of a bunch of other studies being made to enable their use.

Acknowledgments

The authors gratefully acknowledge the financial support of CNPq (Project 167982/2018—4) and Fundação Carlos Chagas Filho de Amparo à Pesquisa do Estado do Rio de Janeiro (FAPERJ-E-26/201.315/2021). We also acknowledge Fundação de Amparo à Pesquisa do Maranhão—FAPEMA—and Coordenação de Aperfeiçoamento de Pessoal de Nível Superior—CAPES—Financial support 001. N. E-C. Maluf and A.G.M da Silva thank them for their CNPq fellowships (#142339/2016—4 and # 308322/2022—3). Maitê Gothe acknowledges, for her PhD grant, FAPESP and SHELL Brazil through the 'Research Centre for Gas Innovation—RCGI' (FAPESP Project 2014/50279-4).

Conflicts of interest

There are no conflict of interest to declare.

References

[1] Liu, L.; Tai, X.; Zhou, X.; Hou, J.; Zhang, Z. Bimetallic Au–Ni Alloy Nanoparticles in a Metal–organic framework (MIL-101) as Efficient Heterogeneous Catalysts for Selective Oxidation of Benzyl Alcohol into Benzaldehyde. *J. Alloys Compd.* **2019**, *790*, 326–336. https://doi.org/10.1016/j.jallcom.2019.03.186.

[2] Cattaneo, S.; Althahban, S.; Freakley, S. J.; Sankar, M.; Davies, T.; He, Q.; Dimitratos, N.; Kiely, C. J.; Hutchings, G. J. Synthesis of Highly Uniform and Composition-Controlled Gold–Palladium Supported Nanoparticles in Continuous Flow. *Nanoscale* **2019**, *11*, 8247–8259. https://doi.org/10.1039/C8NR09917K.

[3] Chowdhury, R.; Mollick, M. M. R.; Biswas, Y.; Chattopadhyay, D.; Rashid, M. H. Biogenic Synthesis of Shape-Tunable Au-Pd Alloy Nanoparticles with Enhanced Catalytic Activities. *J. Alloys Compd.* **2018**, *763*, 399–408. https://doi.org/10.1016/j.jallcom.2018.05.343.

[4] Li, F.; Luo, M. Defect-Rich Ni-Ti Layered Double Hydroxide as a Highly Efficient Support of Au Nanoparticles for Base-Free and Solvent-Free Selective Oxidation of Benzyl Alcohol. *Dalton Trans.* **2018**, *47*, 4056–4067. https://doi.org/10.1039/C7DT04229A.

[5] Marelli, M.; Jouve, A.; Villa, A.; Psaro, R.; Balerna, A.; Prati, L.; Evangelisti, C. Hybrid Au/CuO Nanoparticles: Effect of Structural Features for Selective Benzyl Alcohol Oxidation. *J. Phys. Chem. C* **2019**, *123*, 2864–2871. https://doi.org/10.1021/acs.jpcc.8b09449.

[6] Khawaji, M.; Zhang, Y.; Loh, M.; Graça, I.; Ware, E.; Chadwick, D. Composition Dependent Selectivity of Bimetallic Au-Pd NPs Immobilised on Titanate Nanotubes in Catalytic Oxidation of Glucose. *Appl. Catal. B* **2019**, *256*, 117799. https://doi.org/10.1016/j.apcatb.2019.117799.

[7] Haruta, M. Novel Gold Catalysts for the Oxidation of Carbon Monoxide at a Temperature Far below 0 °C. *Chem. Lett.* **1987**, *16*, 405–408.
[8] Haruta, M. Gold Catalysts Prepared by Coprecipitation for Low-Temperature Oxidation of Hydrogen and of Carbon Monoxide. *J. Catal.* **1989**, *115*, 301–309. https://doi.org/10.1016/0021-9517(89)90034-1.
[9] Nkosi, B.; Coville, N. J.; Hutchings, G. J. Reactivation of a Supported Gold Catalyst for Acetylene Hydrochlorination. *J. Chem. Soc., Chem. Commun.* **1988**, 71. https://doi.org/10.1039/c39880000071.
[10] Prati, L.; Rossi, M. Gold on Carbon as a New Catalyst for Selective Liquid Phase Oxidation of Diols. *J. Catal.* **1998**, *176*, 552–560. https://doi.org/10.1006/jcat.1998.2078.
[11] Porta, F.; Prati, L.; Rossi, M.; Coluccia, S.; Martra, G. Metal Sols as a Useful Tool for Heterogeneous Gold Catalyst Preparation: Reinvestigation of a Liquid Phase Oxidation. *Catal. Today* **2000**, *61*, 165–172. https://doi.org/10.1016/S0920-5861(00)00370-9.
[12] Carrettin, S.; McMorn, P.; Johnston, P.; Griffin, K.; Kiely, C. J.; Hutchings, G. J. Oxidation of Glycerol Using Supported Pt, Pd and Au Catalysts. *Phys. Chem. Chem. Phys.* **2003**, *5*, 1329–1336. https://doi.org/10.1039/b212047j.
[13] Biella, S.; Prati, L.; Rossi, M. Selectivity Control in the Oxidation of Phenylethane-1,2-Diol with Gold Catalyst. *Inorg. Chim. Acta* **2003**, *349*, 253–257. https://doi.org/10.1016/S0020-1693(03)00040-9.
[14] Tareq, S.; Yap, Y. H. T.; Saleh, T. A.; Abdullah, A. H.; Rashid, U.; Saiman, M. I. Synthesis of Bimetallic Gold-Pallidum Loaded on Carbon as Efficient Catalysts for the Oxidation of Benzyl Alcohol into Benzaldehyde. *J. Mol. Liq.* **2018**, *271*, 885–891. https://doi.org/10.1016/j.molliq.2018.09.037.
[15] Silva, T. A. G.; Landers, R.; Rossi, L. M. Magnetically Recoverable AuPd Nanoparticles Prepared by a Coordination Capture Method as a Reusable Catalyst for Green Oxidation of Benzyl Alcohol. *Catal. Sci. Technol.* **2013**, *3*, 2993. https://doi.org/10.1039/c3cy00261f.
[16] Kaizuka, K.; Miyamura, H.; Kobayashi, S. Remarkable Effect of Bimetallic Nanocluster Catalysts for Aerobic Oxidation of Alcohols: Combining Metals Changes the Activities and the Reaction Pathways to Aldehydes/Carboxylic Acids or Esters. *J. Am. Chem. Soc.* **2010**, *132*, 15096–15098. https://doi.org/10.1021/ja108256h.
[17] Wang, D.; Villa, A.; Porta, F.; Prati, L.; Su, D. Bimetallic Gold/Palladium Catalysts: Correlation between Nanostructure and Synergistic Effects. *J. Phys. Chem. C* **2008**, *112*, 8617–8622. https://doi.org/10.1021/jp800805e.
[18] Wu, L.; Wang, Z. The Cooperation Effect in the Au-Pd/LDH for Promoting Photocatalytic Selective Oxidation of Benzyl Alcohol. *Catal. Sci. Technol.* **2017**, *7*, 3771–3773. https://doi.org/10.1039/C7CY02006F.
[19] Wang, R.; Li, B.; Xiao, Y.; Tao, X.; Su, X.; Dong, X. Optimizing Pd and Au-Pd Decorated Bi2WO6 Ultrathin Nanosheets for Photocatalytic Selective Oxidation of Aromatic Alcohols. *J. Catal.* **2018**, *364*, 154–165. https://doi.org/10.1016/j.jcat.2018.05.015.
[20] Sha, J.; Paul, S.; Dumeignil, F.; Wojcieszak, R. Au-Based Bimetallic Catalysts: How the Synergy between Two Metals Affects Their Catalytic Activity. *RSC Adv.* **2019**, *9*, 29888–29901. https://doi.org/10.1039/C9RA06001D.
[21] Rucinska, E.; Pattisson, S.; Miedziak, P. J.; Brett, G. L.; Morgan, D. J.; Sankar, M.; Hutchings, G. J. Cinnamyl Alcohol Oxidation Using Supported Bimetallic Au–Pd Nanoparticles: An Optimization of Metal Ratio and Investigation of the Deactivation Mechanism Under Autoxidation Conditions. *Top. Catal.* **2020**, *63*, 99–112. https://doi.org/10.1007/s11244-020-01231-0.
[22] JamJam, N. M.; Taufiq Yap, Y. H.; Muhamad, E. N.; Izham Saiman, M.; Saleh, T. A. Free Solvent Oxidation of Molecular Benzyl Alcohol by Newly Synthesized AuPd/Titania Catalysts. *Inorg. Chem. Commun.* **2019**, *107*, 107471. https://doi.org/10.1016/j.inoche.2019.107471.
[23] Chen, S.-S.; Yang, Z.-Z.; Wang, A.-J.; Fang, K.-M.; Feng, J.-J. Facile Synthesis of Bimetallic Gold-Palladium Nanocrystals as Effective and Durable Advanced Catalysts for Improved Electrocatalytic Performances of Ethylene Glycol and Glycerol Oxidation. *J. Colloid Interface Sci.* **2018**, *509*, 10–17. https://doi.org/10.1016/j.jcis.2017.08.063.
[24] Gogoi, N.; Borah, G.; Gogoi, P. K.; Chetia, T. R. TiO_2 Supported Gold Nanoparticles: An Efficient Photocatalyst for Oxidation of Alcohol to Aldehyde and Ketone in Presence of Visible Light Irradiation. *Chem. Phys. Lett.* **2018**, *692*, 224–231. https://doi.org/10.1016/j.cplett.2017.12.015.
[25] Song, H. M.; Anjum, D. H.; Sougrat, R.; Hedhili, M. N.; Khashab, N. M. Hollow Au@Pd and Au@Pt Core–Shell Nanoparticles as Electrocatalysts for Ethanol Oxidation Reactions. *J. Mater. Chem.* **2012**, *22*, 25003. https://doi.org/10.1039/c2jm35281h.
[26] Zhong, R.-Y.; Sun, K.-Q.; Hong, Y.-C.; Xu, B.-Q. Impacts of Organic Stabilizers on Catalysis of Au Nanoparticles from Colloidal Preparation. *ACS Catal.* **2014**, *4*, 3982–3993. https://doi.org/10.1021/cs501161c.

[27] Oumahi, C.; Lombard, J.; Casale, S.; Calers, C.; Delannoy, L.; Louis, C.; Carrier, X. Heterogeneous Catalyst Preparation in Ionic Liquids: Titania Supported Gold Nanoparticles. *Catal. Today* **2014**, *235*, 58–71. https://doi.org/10.1016/j.cattod.2014.03.029.

[28] Somsri, S.; Prasertsab, A.; Pornsetmetakul, P.; Maineawklang, N.; Nguyen, M. T.; Yonezawa, T.; Wattanakit, C. Synthesis of Cyclodextrin-Stabilized Gold Nanoparticles Supported Hierarchical Zeolites for the Facile Production of Furandicarboxylic Acid (FDCA) from 5-Hydroxymethylfurfural (HMF). *Microporous Mesoporous Mater.* **2023**, *354*, 112559. https://doi.org/10.1016/j.micromeso.2023.112559.

[29] Shang, L.; Liang, Y.; Li, M.; Waterhouse, G. I. N.; Tang, P.; Ma, D.; Wu, L.-Z.; Tung, C.-H.; Zhang, T. "Naked" Magnetically Recyclable Mesoporous Au-γ-Fe_2O_3 Nanocrystal Clusters: A Highly Integrated Catalyst System. *Adv. Funct. Mater.* **2017**, *27*, 1606215. https://doi.org/10.1002/adfm.201606215.

[30] Silva, T. A. G.; Ferraz, C. P.; Gonçalves, R. V.; Teixeira-Neto, E.; Wojcieszak, R.; Rossi, L. M. Restructuring of Gold-Palladium Alloyed Nanoparticles: A Step towards More Active Catalysts for Oxidation of Alcohols. *ChemCatChem* **2019**, *11*, 4021–4027. https://doi.org/10.1002/cctc.201900553.

[31] Cybula, A.; Priebe, J. B.; Pohl, M.-M.; Sobczak, J. W.; Schneider, M.; Zielińska-Jurek, A.; Brückner, A.; Zaleska, A. The Effect of Calcination Temperature on Structure and Photocatalytic Properties of Au/Pd Nanoparticles Supported on TiO_2. *Appl. Catal. B* **2014**, *152–153*, 202–211. https://doi.org/10.1016/j.apcatb.2014.01.042.

[32] Pereira, L.; Ribeiro, C.; Tofanello, A.; Costa, J.; De Moura, C.; Garcia, M.; De Moura, E. Gold Supported on Strontium Surface-Enriched $CoFe_2O_4$ Nanoparticles: A Strategy for the Selective Oxidation of Benzyl Alcohol. *J. Braz. Chem. Soc.* **2019**. https://doi.org/10.21577/0103-5053.20190030.

[33] Xiaoxiang, H.; Yingying, K.; Chunhua, X.; Xiujuan, T.; Qing, C.; Kuiwu, W.; Chin-Te, H.; Li-Li, L.; Shang-Bin, L. Heteropoly Tungstate Supported on Metal Oxide Catalysts for Liquid Phase Oxidation of Benzyl Alcohol with Hydrogen Peroxide. *J. Braz. Chem. Soc.* **2017**. https://doi.org/10.21577/0103-5053.20170117.

[34] Wang, Z.; Zhang, B.; Yang, S.; Yang, X.; Meng, F.; Zhai, L.; Li, Z.; Zhao, S.; Zhang, G.; Qin, Y. Dual Pd^{2+} and Pd^0 Sites on CeO_2 for Benzyl Alcohol Selective Oxidation. *J. Catal.* **2022**, *414*, 385–393. https://doi.org/10.1016/j.jcat.2022.09.012.

[35] Crombie, C. M.; Lewis, R. J.; Taylor, R. L.; Morgan, D. J.; Davies, T. E.; Folli, A.; Murphy, D. M.; Edwards, J. K.; Qi, J.; Jiang, H.; et al. Enhanced Selective Oxidation of Benzyl Alcohol via In Situ H_2O_2 Production over Supported Pd-Based Catalysts. *ACS Catal.* **2021**, *11*, 2701–2714. https://doi.org/10.1021/acscatal.0c04586.

[36] Yamada, L. K.; da Silva, A. G. M.; Rodrigues, T. S.; Haigh, S. J.; Camargo, P. H. C. Bimetallic Au@Pd-Au Tadpole-Shaped Asymmetric Nanostructures by a Combination of Precursor Reduction and Ostwald Ripening. *ChemNanoMat* **2016**, *2*, 509–514. https://doi.org/10.1002/cnma.201600049.

[37] Li, C.; Li, D.; Wan, G.; Xu, J.; Hou, W. Facile Synthesis of Concentrated Gold Nanoparticles with Low Size-Distribution in Water: Temperature and pH Controls. *Nanoscale Res. Lett.* **2011**, *6*, 440. https://doi.org/10.1186/1556-276X-6-440.

Supplementary Materials

Table S1. Central composite design table with response values

	Calcination Temperature / °C	Reaction Temperature / °C	Benzyl Alcohol Conversion / %	Benzaldehyde Selectivity / %
Simple factorial design	200.00	60.00	0.55	100.00
	500.00	60.00	0.53	100.00
	200.00	120.00	48.84	84.16
	500.00	120.00	51.51	80.65
Central points	350.00	90.00	2.39	100.00
	350.00	90.00	2.31	100.00
	350.00	90.00	2.69	98.13
Alpha points	137.87	90.00	3.20	95.68
	562.13	90.00	4.73	93.20
	350.00	47.57	0.51	100.00
	350.00	132.43	90.30	57.84

Table S2. Surface analysis of $AuPd/SiO_2$ catalysts

Catalyst	Area / $m^2\ g^{-1}$	Pore Volume / $cm^3\ g^{-1}$
As prepared	369	0.77
Calcined at 562 °C	232	0.58

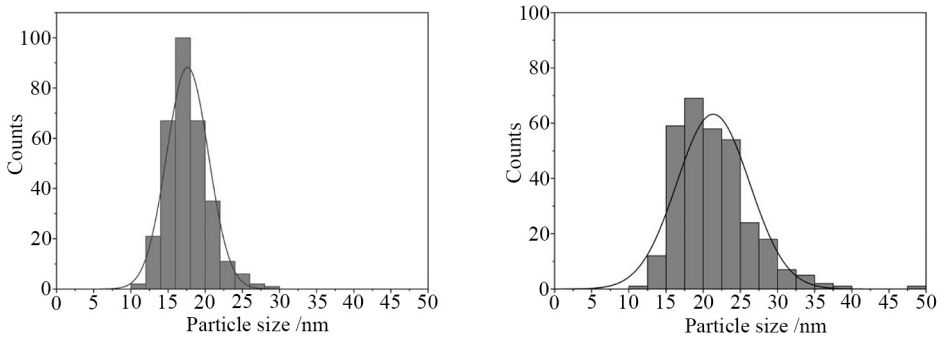

Figure S1. Histograms of nanoparticle size distribution. On the left side, the as-prepared catalyst, and on the right side, the catalyst calcined at 562 °C

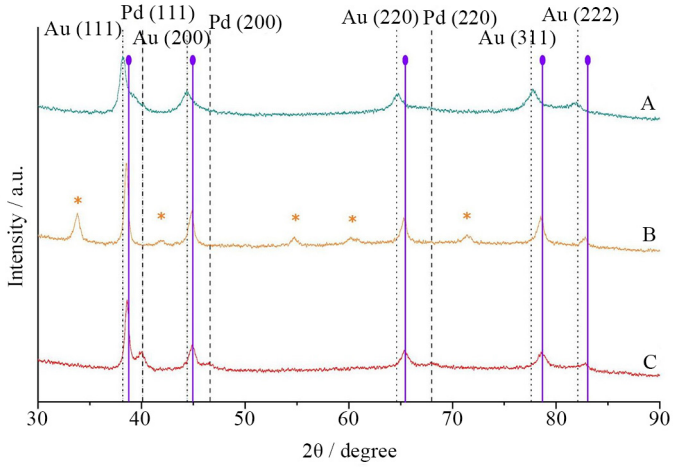

Figure S2. XRD patterns of catalyst $AuPd/SiO_2$ (A) as prepared (B) calcined in air at 562 °C and (C) calcined in air at 562 °C and treated with H_2 at 100 °C. $Au_{1.51}Pd_{0.49}$ alloy reference peaks are marked with ●, and PdO species are marked with *

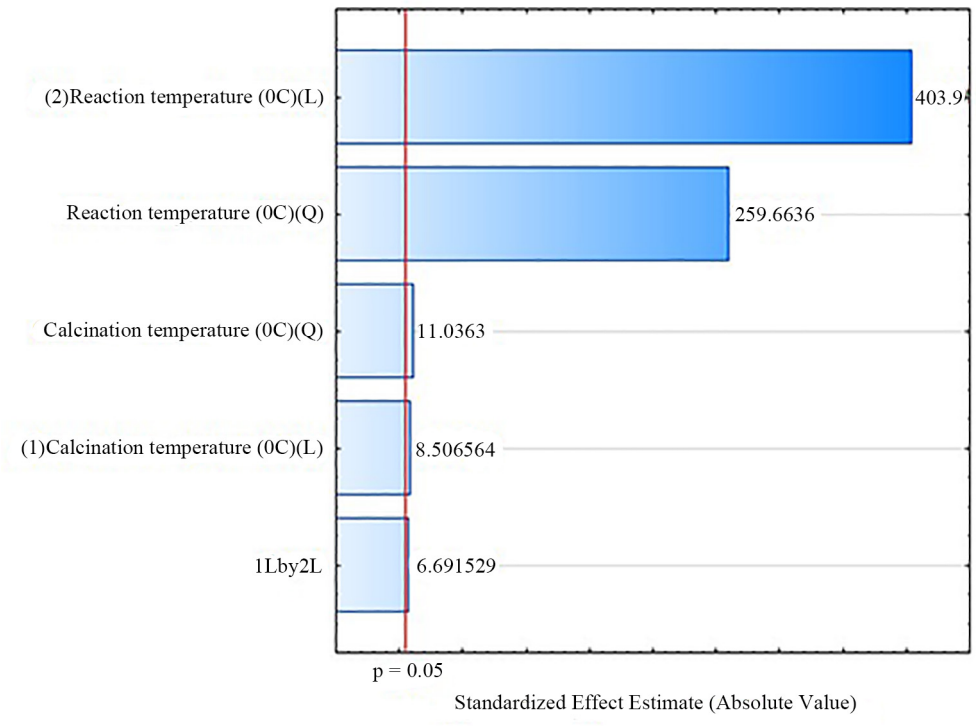

Figure S3. Pareto Chart of Standardized Effects in the conversion of benzyl alcohol

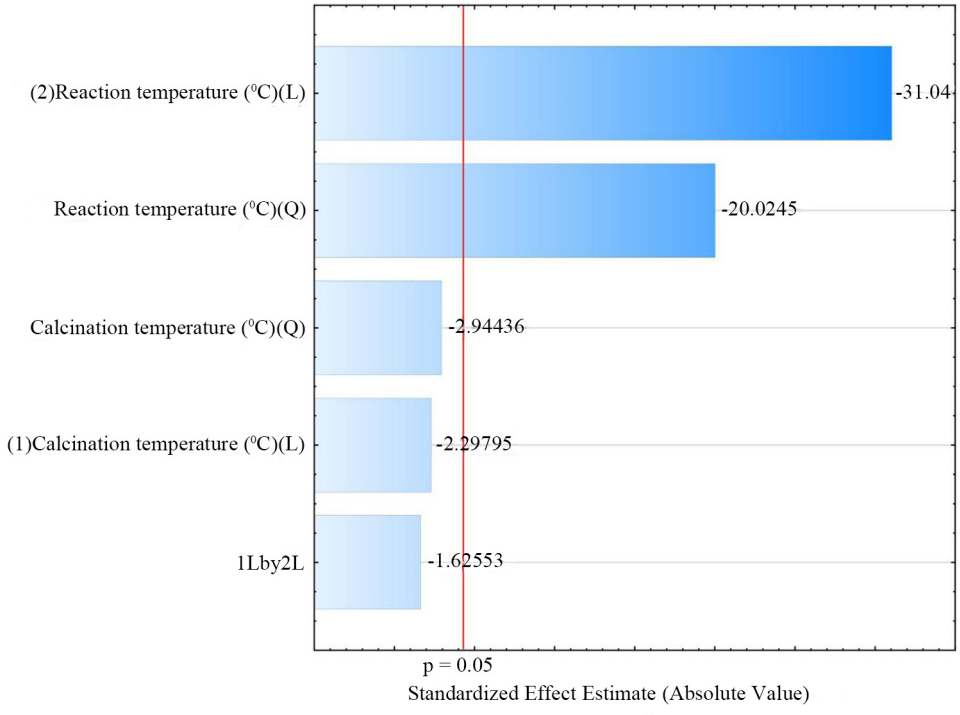

Figure S4. Pareto Chart of Standardized Effects in selectivity to benzaldehyde

Table S3. ANOVA table for the benzyl alcohol conversion

Variation Factor	Quadratic Sum	Degrees of Freedom	Quadratic Mean	F
Regression error	9230.98	5	1846.2	95.15
Residual error	97.01	5	19.4	
Lack of Fit	96.93	3	32.31	807.75
Pure error	0.08	2	0.04	
Total	9327.99	10		

Table S4. Regression coefficients table for the benzyl alcohol conversion

Factor	Regression Coefficient	*p*-Value
Mean/Interc.	120.62885	0.000092
Calcination temperature / L	−0.03790	0.007479
Calcination temperature / Q	0.00004	0.008110
Reaction temperature / L	−3.43688	0.000029
Reaction temperature / Q	0.02405	0.000015
1L by 2L	0.00015	0.021612

Table S5. ANOVA table for the benzaldehyde selectivity

Variation Factor	Quadratic Sum	Degrees of Freedom	Quadratic Mean	F
Regression error	1611.4	2	805.7	54.69
Residual error	117.86	8	14.73	
Lack of Fit	115.53	6	19.25	16.52
Pure error	2.33	2	1.17	
Total	1729.26	10		

Table S6. Regression coefficients table for the benzaldehyde selectivity

Factor	Regression Coefficient	*p*-Value
Mean/Interc.	41.67338	0.022238
Calcination temperature / L	0.05332	0.097267
Calcination temperature / Q	−0.00006	0.098587
Reaction temperature / L	1.49274	0.004538
Reaction temperature / Q	−0.01011	0.002485
1L by 2L	−0.00020	0.245557

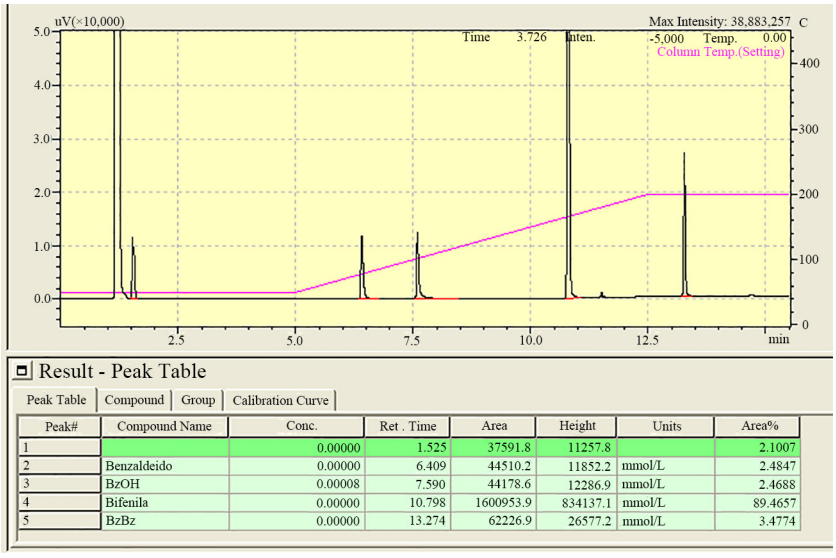

Figure S5. GC-FID image example obtained from the experiments